Sintering of Ni-Zn Ferrite Nanopowders By the
Constant Heating Rate (Chr) Method

Ana Cristina Figueiredo de Melo Costa[a]*, *Edener Tortella*[b], *Elias Fagury Neto*[b],

Márcio Raymundo Morelli[b], *Ruth Herta Goldschmidt Aliaga Kiminami*[b]

[a]*Department of Materials Eng., Federal University of Campina Grande,*
58109 - 970 Campina Grande - SP, Brazil
[b]*Department of Materials Eng., Federal University of São Carlos,*
13565-905 São Carlos - SP, Brazil

The constant heating rate method employed in sintering studies offers several advantages over the isothermal method, particularly the fact that all the parameters that describe the sintering phenomena can be obtained from a single sample. The purpose of this work is to determine the parameters of sintering kinetics of nanosized Ni-Zn ferrite powders synthesized by combustion reaction. The nonisothermal sintering method was studied using a constant heating rate (CHR). The Ni-Zn ferrite powders, with average particle size varying from 18 nm to 29 nm, were uniaxially pressed and sintered in an horizontal dilatometer at a constant heating rate of 5.0 °C/min from 600 °C up to complete densification, which was reached at 1200 °C. The compacts were characterized by scanning electron microscopy (SEM). Experimental results revealed three different sintering stages, which were identified through the Bannister Theory. The shrinkage and the shrinkage rate analyzed showed a viscous contribution in the initial sintering stage, which was attributed to the mechanism of structural nanoparticle rearrangement.

1. Introduction

The sintering of ferrites via solid state, as well as of other ceramic materials, is a thermal process that causes reduction of the surface area through the formation of grain boundaries, neck growth between particles and usually also densification. During the solid state sintering process, the porosity decreases and the material's microstructure, which defines the performance of the final product, is developed. The sintering stages represent the geometrical evolution that occurs during the transformation of a compact powder into a dense and resistant solid[1,2]. During these stages, the overall interface free energy of a set of particles decreases because the reduction of solid-vapor interface energy is greater than the increase of solid-solid interface energy (grain boundary) of the system[3]. The driving force of the sintering process is the reduction of overall free energy by the decrease of specific surface area and compact interfaces. Solid state sintering may be performed by two alternative processes: densification, with a change of the solid-vapor interface

(particle-pore) into solid-solid interface with less energy, or grain growth, with the transformation of numerous small grains (the compact's particles) into a smaller number of large grains. From this standpoint, therefore, the microstructural changes that occur during solid sate sintering result from the combined effect of densification and grain growth[4].

The sintering kinetics of ceramic materials was investigated here using the nonisothermal method, i.e., the constant heating rate (TCA or CHR). Compared to conventional isothermal sintering, this method yields faster results and requires only one sample, also allowing for an examination of the entire sintering history[5]. The nonisothermal techniques for analysis of the sintering stage initially allow for the determination of sintering parameters such as the sintering coefficient, activation energy and diffusion sintering[6]. Starting from the basic sintering equation, Woolfrey and Bannister[7,8] proposed a series of Arrhenius-like equations for the study of constant heating

*e-mail: anacristina@dema.ufcg.edu.br

rate (CHR) sintering, suggesting the following equation:

$$T^2 \frac{d}{dt}\left(\frac{\Delta L}{L_o}\right) = \left(\frac{Q}{(n+1)R}\right)\left(\frac{\Delta L}{L_o}\right) \qquad (1)$$

where T is the temperature (K), $d((\Delta L/L_o)/dt$ is the linear shrinkage differential, $\Delta L/L_o$ is the linear shrinkage (%), Q is the activation energy (kJ/mol), R is the ideal gas constant (J/mol.K), and n is the sintering mechanism. Based on Eq. 1, a $T^2 d(\Delta L/L_o)/dt$ vs. $(\Delta L/L_o)$ plot should consist of a straight line with an angular coefficient $Q/(n+1)R$, in which $Q/(n+1)$ may be calculated. In order to obtain the n value, the activation energy Q must be calculated by the Dorn method[9]. Once Q has been calculated, n can be determined and the sintering mechanism, which acts in the sintering stages, identified as shown in Table 1.

Several current scientific research efforts in the field of ceramic technology of ferrites by solid-state reaction study these materials, behavior during sintering by attempting to gain a better understanding of the mechanisms and phenomena involved in grain densification and growth. This knowledge is important to allow changes in the composition and processing of ferrites to be effected, with the purpose of obtaining microstructures that confer on the sintered material properties and characteristics appropriate for their application. Some of these studies are the following: Levesque[10] and Paulus[11,12] studied the grain growth of Mn-Zn ferrites in the early stage of sintering; Jain *et al.*[13] reported on grain growth kinetics in the intermediate stage of Mn-Zn-Fe ferrite sintering, which was obtained by the conventional oxide blending method. The activation energy determined for the intermediate stage was 130 Kcal/mol; Dias *et al.*[3] investigated the sintering kinetics of the intermediate and final stages of Ni-Zn ferrites prepared by hidrothermal synthesis; Parvatheeswara Rao *et al.*[14] studied the evolution of Ni-Zn ferrite microstructures at sintering temperatures in the range of 1150 ° to 1300 °C for 1 to 4 h. Densification and grain growth was reported as Arrhenius rate controlled processes with activation energies of 63.9 and 64.4 Kcal/mol, respectively. Cho *et al.*[15] investigated the behavior during sintering of nanocrystalline Ni-Zn ferrites, chemically modified by the addition of Si and Ca. The activation energy estimated for grain boundary

Table 1. Sintering mechanism according to Wooffrey and Bannister[7,8].

n	Sintering Mechanism
0	Viscous flow
1	Bulk diffusion
2	Grain boundary diffusion

diffusion was 310 kJ/mol and 470 kJ/mol, respectively, for Ni-Zn ferrites with and without additives. An activation energy of 750 kJ/mol was calculated for micrometric Ni-Zn ferrite powders.

The above-mentioned studies investigated the sintering kinetics throughout the sintering stages of this material. However, no reports appear to be available regarding specific research work on the sintering kinetics of $Ni_{0.7}Zn_{0.3}Fe_2O_4$ ferrites synthesized by combustion reaction. Hence, by means of the nonisothermal, constant heating rate (CHR) method, this study aimed to evaluate the effect of Zn^{2+} concentrations on the sintering kinetics of $Ni_{1-x}Zn_xFe_2O_4$ nanometric powder with x = 0.3; 0.5; 0.7% mol of Zn^{2+} obtained by combustion reaction.

2. Experimental

To synthesize ferrite powders by combustion reaction, $Ni(NO_3)_2.6H_2O$, $Zn(NO_3)_2.6H_2O$, and $Fe(NO_3)_3.9H_2O$ were used as precursor reagents (oxidizing agents) and cation sources and urea $(CO(NH_2)_2)$ as the reducing agent. The procedure used to synthesize the powders by combustion reaction has been described in detail in previous reports[16,18]. Powders with particle sizes ranging from 18 to 29 nm were compacted into 9.8 mm diameter, 3 mm high pellets by uniaxial pressing at 385 MPa (green density 59.1 ± 0.98 of theoretical density). The samples, which were named C03, C05 and C07 for systems with 0.3, 0.5 and 0.7% mol of Zn^{2+}, respectively, were calcined at 600 °C/1h for binder burnout (5% PVAL) and then sintered at 1200 °C in a NETZCHS 402E dilatometer at a constant heating rate of 5 °C/min. After sintering, the samples were polished with 0.3 µm alumina, thermally etched at 1100 °C for 30 min, and then analyzed by SEM (XL30 FEG, Philips). Representative micrographs of the samples were used to determine the mean grain size using the MOCHA software program (Jandel, Image Analyzer).

3. Results and Discussion

The early, intermediate and final stages of Ni-Zn ferrite sintering were evaluated to investigate the effect of the concentration of Zn^{2+} on the sintering of nanometric powders of Ni-Zn ferrites synthesized by combustion reaction. Figs. 1a and b and Table 2 show the results obtained for linear shrinkage $(\Delta L/L_0)$ and linear shrinkage rate $(d(\Delta L/L_0)/dt)$ according to temperature, for systems C03, C05 and C07, which corresponded, respectively, to 0.3, 0.5 and 0.7 mol of Zn^{2+}. Increases in the concentration of Zn^{2+} affected the sintering behavior, reducing the linear shrinkage at the point of maximum linear shrinkage and final density of the samples. The C03 and C05 systems displayed similar values of temperature at the

maximum linear shrinkage rate (1016 °C), although the C05 system showed a lower maximum linear shrinkage rate (1.9E-1 1/min) than the C03 system (3.3E-1 1/min).

The temperature for the onset of retraction (814 °C) was found to be higher in the C07 system than in the C03 and C05 (787 °C and 763 °C) systems. On other hand, the temperature at the point of maximum linear shrinkage (978 °C) for C07 was lower than in the other systems (1016 °C). The point of maximum linear shrinkage decreased according to the Zn^{2+} concentration in the system; in other words, the shrinkage in the C07 system

(0.7% mol of Zn^{2+}) was 5.86% (73.1% of theoretical density), whereas it was 8.08% (72,21% of theoretical density) in the C05 system and 9.96% (81.72% of theoretical density) in the C03 system. The same behavior was observed for retraction at the final temperature (1200 °C), i.e., 11.88% (89.13% of theoretical density), 13.68% (93.23% of theoretical density) and 14.48% (95.38% of theoretical density), respectively, for the C07, C05 and C03 systems.

Figure 2 shows the plot calculated by Woolfrey and Bannister's method[7,8], to determine the sintering coeffi-

Table 2. Results of sintering at 1200 °C for the C03, C05 and C07 systems with a constant heating rate of 5 °C/min.

Systems	C03 $Ni_{0.7}Zn_{0.3}Fe_2O_4$	C05 $Ni_{0.5}Zn_{0.5}Fe_2O_4$	C07 $Ni_{0.3}Zn_{0.7}Fe_2O_4$
Starting shrinkage temperature (°C)	787	763	814
Temperature at the point of maximum linear shrinkage (°C)	1016	1016	978
Shrinkage rate at the point of maximum linear shrinkage rate (1/min)	3.35E-1	1.93E-1	2.22E-1
Shrinkage at the point of maximum linear shrinkage rate (%)	9.96	8.08	5.86
Linear shrinkage at the point of maximum linear shrinkage rate (%)	81.72	77.21	73.10
Linear shrinkage at 1200 °C (%)	14.48	13.68	11.88
Relative density at 1200 °C (%)	95.38	93.23	89.13
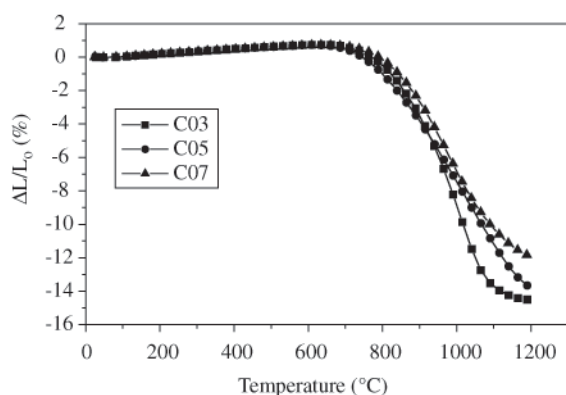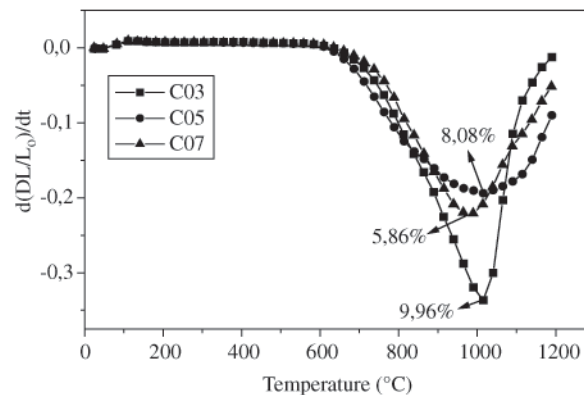
(a)   (b)

Figure 1. Sintering results obtained for the C03, C05 and C07 systems; a) linear shrinkage, b) linear shrinkage rate, both in terms of temperature, with a constant heating rate of 5 °C/min.

cients with a constant heating rate (CHR) of 5 °C/min, for the early, intermediate and final stages. The activation energy was determined by the Dorn method[9]. Table 3 shows the values of activation energy and sintering coefficients for the three stages of sintering. The linear part of the curve represents the stages in which probably only one sintering mechanism took place, while the nonlinear part represents a transition region between two mechanisms.

The initial stage developed to 2.5% in the three systems investigated. The activation energy values ranged from 214.61 to 242.70 and the sintering mechanism was $n \sim 0$, indicating that the prevailing mechanism in the initial stage of sintering in the three systems was structural rearrangement of nanoparticles, with viscous flow characteristics ($n = 0$). The activation energy values were lower than those estimated by Cho *et al.*[15] for grain boundary diffusion, which were 310 kJ/mol and 470 kJ/mol for Mn-Zn ferrite nanopowders.

The second stage ranged from 3.0% to 10.0% in C03, 3.0% to 8.0% in C05, and 3.0% to 6.0% in C07. It was found, in this stage, that the nanoparticles also simulated a viscous

Figure 2. $T^2(\Delta L/L_o)/dt$ *vs.* $\Delta L/L_o$ calculated through Bannister's equation. for systems C03, C05 and C07 with a constant heating rate of 5 °C/min.

flow behavior, as in the initial stage, owing to the presence of nanoparticles. However, grain boundary diffusion was believed to take place in this stage. The activation energy showed coherent values corresponding to the intermediate stage. In C03 and C05, these values (130kJ/mol) were lower than those proposed by Jain *et al.*[13] for the sintering of Mn-Zn ferrites; nevertheless, C07 presented very similar values.

The third stage corresponded to the point of maximum linear shrinkage, coarsening, and decrease of the linear shrinkage rate due to a decrease of surface free energy. This stage ended when the final temperature was reached (1200 °C). It was observed that the primary mechanism was bulk diffusion ($n = 1.0$), owing to the nanometric size of the particles. Linear shrinkage rates of 9.96, 8.08 and 5.86% corresponded to the point of maximum linear shrinkage of C03, C05 and C07, respectively (Table 2). The activation energy presented typical values for this stage, ranging from 35.22 kJ/mol to 45.06 kJ/mol.

Figures 3, 4 and 5 depict the sintering process of C03, C05 and C07 through SEM micrographs. Figures 3a, 3b and 3c show the linear shrinkage ($\Delta L/L_0$) at 800 °C (initial stage) for C03, C05 and C07, which correspond to the following linear shrinkage hates: 0.58; 1.15; and 0.23%, respectively. In this test configuration it was observed that the early stage of neck growth occurred between two particles. This level coincided with the initial stage, in which the structural rearrangement of nanoparticles with a viscous flow characteristic is dominant.

Figures 4a, 4b and 4c show the microstructures of C03, C05 and C07 at 1000 °C, which corresponds to the temperature at which the maximum linear retraction occurred (end of intermediate stage). From this point on, grain growth took place owing to decreasing surface free energy. The linear shrinkage and average grain size found at this temperature were 9.19; 7.52 and 6.89% and 0.17 ± 0.81 μm; 0.18 ± 0.93 μm and 0.19 ± 0.82 μm for C03, C05 and C07, respectively.

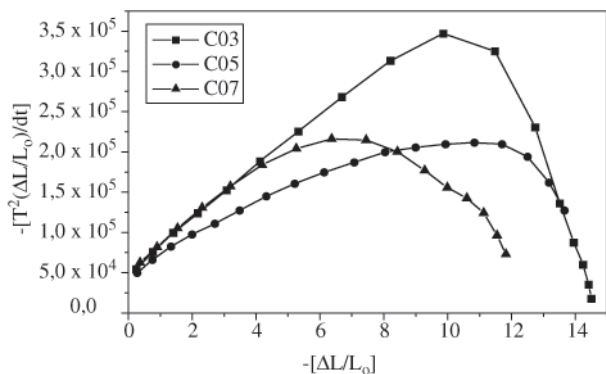Figures 5a, b and c show the microstructures of the systems C03, C05 e C07 at 1100 °C. In this temperature the

Table 3. Sintering parameters with a constant heating rate (CHR) of 5 °C/min for C03, C05 and C07 sintered at 1200 °C; Q = activation energy, n = sintering coefficient.

| Systems	Stages	Q (kJ/mol)	n
C03	Initial	242.70	-0.1877
$Ni_{0.7}Zn_{0.3}Fe_2O_4$	Intermediate	106.65	-0.566
	End	35.44	-1.417
C05	Initial	214.61	-0.1023
$Ni_{0.5}Zn_{0.5}Fe_2O_4$	Intermediate	74.45	-0.3095
	End	35.22	-1.088
C07	initial	224.39	-0.2579
$Ni_{0.3}Zn_{0.7}Fe_2O_4$	Intermediate	136.45	-0.2075
	End	45.06	-1.181

evolution of the grain growth is observed (coarsening) in the final of sintering. The linear shrinkage and the average grain size of certain grain was 13.89; 11.38 and 10.45% and 0.44 ± 0.15 μm; 0.35 ± 0.13 μm and 0.41 ± 0.19 μm for the systems C03, C05 and C07, respectively.
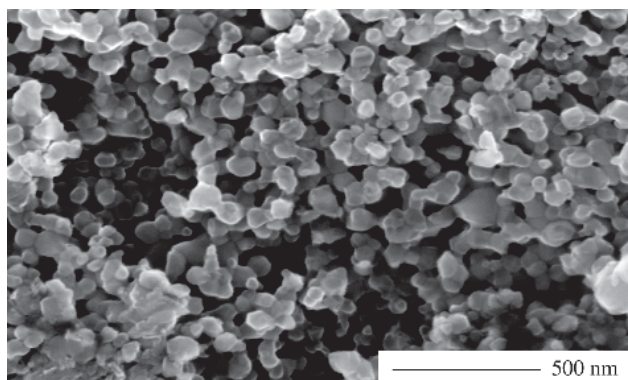
4. Conclusions

Based on the results of the investigation on sintering with a constant heating rate (CHR) reported on herein, the following conclusions were reached: (i) increases in Zn^{2+} content affected the sintering kinetics of Ni-Zn
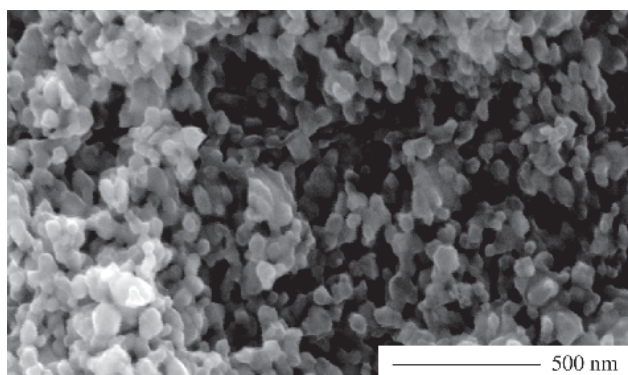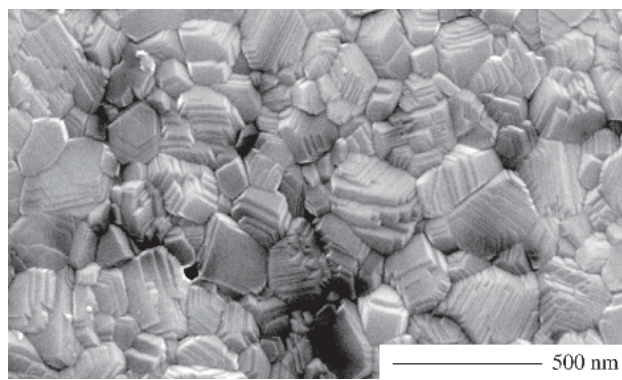

(a)
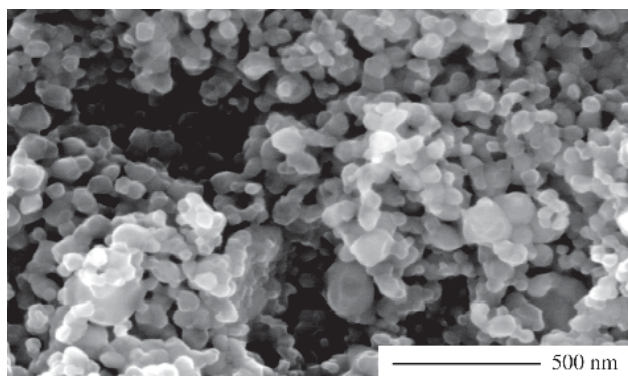
(b)

(c)

Figure 3. SEM Micrographs of a) C03, b) C05, c) C07 at 800 °C, with a CHR of 5 °C/min.
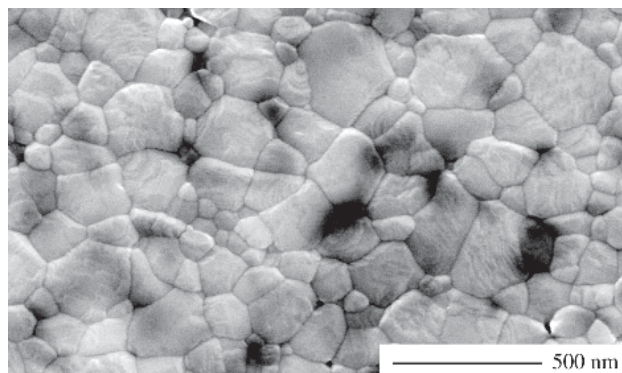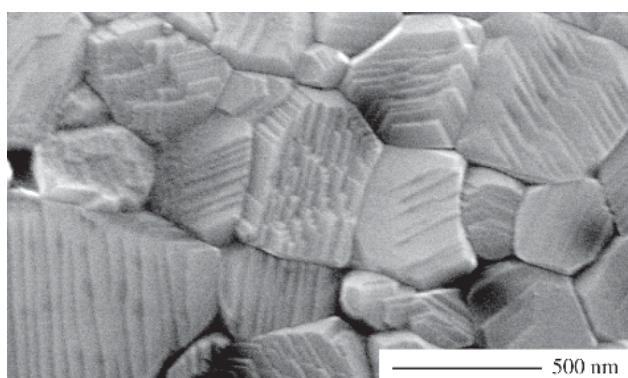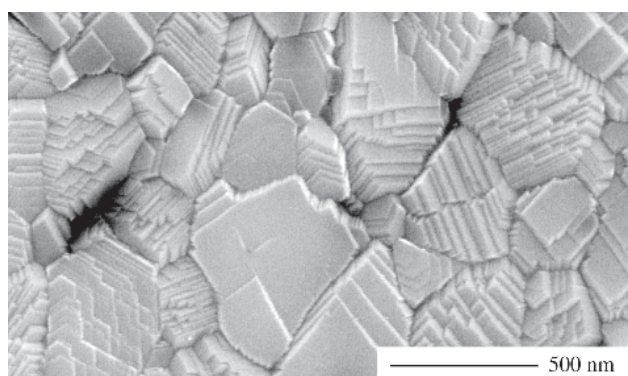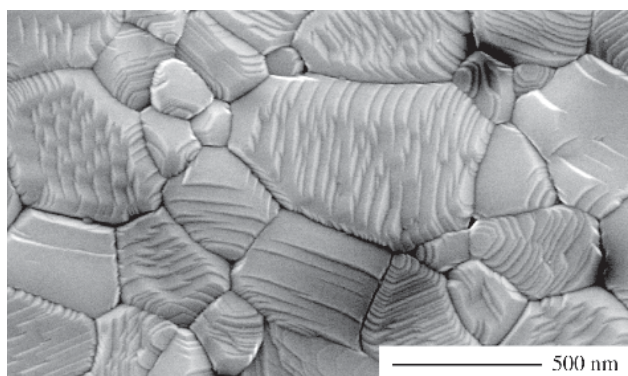

(a)
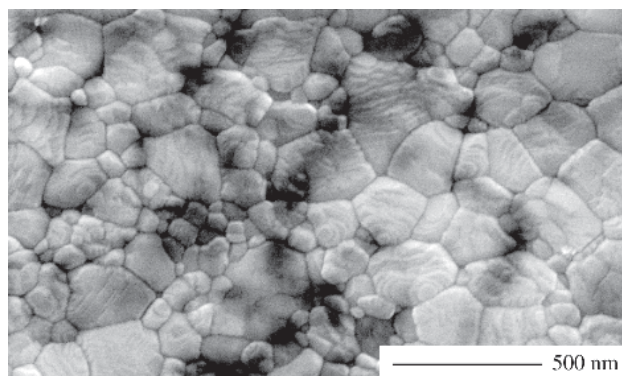
(b)

(c)

Figure 4. SEM Micrographs of: a) C03; b) C05; c) C07 at 1000 °C, with a CHR of 5 °C/min.

(a)

(b)

(c)

Figure 5. SEM micrographs of: a) C03; b) C05; c) C07 at 1100 °C, with a CHR of 5 °C/min.

nanopowders, reducing the maximum densification rate and final density of the samples, but leaving the sintering mechanism unchanged; (ii) the sintering coefficient, calculated for the initial and intermediate stages of the three systems, was n ~ 0, indicating that the predominant mechanism in these stages was structural rearrangement of nanoparticles, with a viscous flow characteristic; (iii) in the final stage, the predominant mechanism governing the sintering of nanopowders in the three systems was bulk diffusion (n ~ 1).

Acknowledgements

References

1. Varela, J.A.; Longo, E. *Cerâmica*, v. 30, n. 172, p. 95-102, 1994.
2. German, R.M. *Sintering Theory and Practice*. Ed. John Wiley & Sons, New York, 1996.
3. Dias, A.; Mohallem, N.D.S.; Moreira, R.L. *Mater. Res. Bull.*, v. 33, n. 3, p. 475-486, 1998.
4. Shaw, N.J. *Advanced ceramics - Powder Metallurgy International*, v. 21, n. 3, p. 16-20, 1989.
5. Leite, E.R.; Longo, E. *Anais do 38º CBC*, v. 1, p. 126-131, 1994.
6. Hillman, S.H.; German, R.M. *J. Mater. Sci.*, v. 27, p. 2641-2648, 1992.
7. Woolfrey, J.L.; Bannister, M.J. *J. Am. Ceram. Soc.*, v. 55, n. 12, p. 390-394, 1972.
8. Woolfrey, J.L. *J. Am. Ceram. Soc.*, v. 55, n. 8, p. 383-388, 1972.
9. Bacmann, J.J.; Cizeron, G. *J. Am. Ceram. Soc.*, v. 51, n. 4, p. 209-212, 1968.
10. Levesque, P.; Gerlach, L.; Zneimer, *J. Am. Ceram. Soc.*, v. 39, n. 3, p. 119-120, 1956.
11. Paulus, M. *Phys. State Solid*, v. 2, p. 1181-1196, 1962.
12. Paulus, M. *Phys. State Solid*, v. 2, p. 1325-1341, 1962.
13. Jain, G.C.; B.K. Das; Goel, N.C. Ind. *J. Pure Appl. Phys.*, v. 14, p. 87-92, 1976.
14. Parvatheeswara Rao, B.; Subba Rao, P.S.V.; Rao, K.H. *J. Phys. IV France*, v. 7, p. C1-241-C1-242, 1997.
15. Cho, Y.S.; Schaffer, D.; Burdick, V.L.; Amarakoon, V.R.W. *Mater. Res. Bull.*, v. 34, n. 14-15, p. 2361-2368, 1999.
16. Costa, A.C.F.M. *et al.*, *J. Mater. Sci.* v. 37, p. 1-4, 2002.
17. Costa, A.C.F.M.; Tortella, E.; Morelli, M. R.; Kiminami R.H.G. A., *J. Metas. and Nanocrys. Mater.*, v. 14, p. 57-64, 2002.
18. Kiminami, R.H.G.A., *KONA Powder and Particle*, v. 19, p. 156-165, 2001.

This article has received corrections in agreement with the ERRATUM published in Volume 8 Number 1.